Impedance Matching and Reradiation in LPTV Receiver Front-Ends: An Analysis Using Conversion Matrices

Sameed Hameed, *Member, IEEE,* and Sudhakar Pamarti, *Member, IEEE*

***Abstract*—Linear periodically time-varying (LPTV) circuits are finding increased prominence in reconfigurable transceiver applications. Impedance matching of such circuits to the antenna impedance is essential for fully on-chip receiver topologies. However, deriving the S_{11} of an LPTV circuit is non-trivial in general. Moreover, reflections at harmonic offsets from input frequencies can also be expected due to the time-varying nature of the circuit. This paper utilizes the conversion matrix-based analysis technique to compute the S_{11} of a general LPTV circuit. Further, it is shown that signal reradiation at harmonic shifts from input frequencies is also obtained as a natural consequence of this analysis. Examples related to mixer-first receivers, switched-capacitor receiver front-ends (with reset) and Filtering-by-Aliasing (FA)-based receivers are considered to verify the analysis. Design guidelines are provided to attain optimal S_{11} in a few such scenarios. Explicit analytical expressions are derived for reradiation in ideal N-path mixer-first receivers and FA-based receivers, while guidelines are provided for proper choice of conversion matrix expressions/sizes in case of numerical computation.**

***Index Terms*—Conversion matrices, LPTV analysis, linear periodically time-varying circuits, programmable receivers, impedance matching, software-defined radio, N-path filters, mixer-first receivers, Filtering-by-Aliasing**

I. Introduction

LINEAR periodically time-varying (LPTV) circuits are linear circuits that have a periodically time-varying impulse response. LPTV circuits are essential due to their ability to frequency-translate the input, and so the mixer, which is the most basic LPTV circuit, is an integral part of wireless transceivers. Due to the recent desire for wide programmability in transceivers, LPTV circuits (such as N-path filters) are being pushed ever-closer to the antenna interface [1]-[6]. In fact, the mixer-first receiver topology directly connects the antenna input to a passive mixer, and achieves high linearity due to the high-Q band-pass impedance realized by the frequency-translation of the baseband input impedance to RF [4]. Other works realize the baseband itself as a time-varying circuit, and integrate it with a mixer to achieve sharp filtering at RF [7], [8]. Thus, understanding the interaction of such LPTV front-ends with an antenna is of the utmost importance.

S. Hameed and S. Pamarti are with the Department of Electrical Engineering, University of California, Los Angeles, CA 90095 USA (e-mail: sameed@ucla.edu; spamarti@ee.ucla.edu).

This work was supported by the U.S. National Science Foundation under Award ECCS 1408647.

Analyzing impedance matching in LPTV circuits is difficult. Further, frequency translations mean that reflections are not confined to input frequencies [4]. As such, analysis is usually handled on a case-by-case basis. For example, some works derive equivalent linear time-invariant (LTI) models of mixer-first receivers using the fact that the voltage on baseband capacitors is relatively constant for input freqiencies close to the switching frequencies [3]-[5]. The LTI-equivalent circuit adds a shunt impedance term, R_{sh}, that reveals the effect of the source impedance on the input impedance of the receiver. Other analysis of current-driven passive mixer circuit approximate the RF current by using the Fourier series of the switch waveforms [9], [10]. This leads to the RF input voltage, and hence input impedance being written as an infinite sum.

General analysis techniques for LPTV circuits start by relating the output, $y(t)$, and the input, $u(t)$, of the system by the convolution, $y(t) = u(t) * h(t, \tau)$, where $h(t, \tau) = \sum_{n=-\infty}^{\infty} h_n(\tau)e^{jn\omega_p t}$ is the periodically time-varying impulse response of the system, and $T_p = 2\pi/\omega_p$ is its period. Taking the Fourier transform of $y(t)$ gives

$$Y(\omega) = \sum_{n=-\infty}^{\infty} H_n(\omega)U(\omega - n\omega_p), \tag{1}$$

where $U(\omega)$ and $Y(\omega)$ are the Fourier transforms of the input and output respectively, and the set of transfer functions, $H_n(\omega) = \widetilde{H}_n(\omega - n\omega_p)$, are known as the *"harmonic transfer functions*" (HTFs) of the LPTV circuit ($\widetilde{H}_n(\omega)$ is the Fourier transform of $h_n(t)$). [11] utilized a state-space approach to solve for the HTFs of a general LPTV circuit, where the circuit is treated as periodically moving through a set of states with each state setting initial conditions for another. [12] extends these methods to provide a unified analysis of samplers and mixers, thereby deriving the HTFs of an N-path switched RC circuit with non-overlapping clocks. The results have been used to derive input impedances in N-path filters [2], and switched-capacitor receivers [13].

More recent works on switched RC circuits focuses on the voltages sampled on the capacitors. [14] derives the signal-flow graph for the operation of a single-path in a switched RC circuit by applying sinusoidal steady-state analysis on the underlying differential equations that is then used to derive driving-point impedance of an N-path structure [15]. In contrast, [16] derives similar results with lower complexity

Table I
CONVERSION MATRIX RELATIONS FOR BASIC LPTV COMPONENTS

Component	LPTV Relation
Resistor	$\underline{V}(\omega) = \mathbb{R}\underline{I}(\omega)$
Capacitor	$\underline{I}(\omega) = j\mathbb{C}\mathbf{\Omega}(\omega)\underline{V}(\omega)$
Inductor	$\underline{V}(\omega) = j\mathbb{L}\mathbf{\Omega}(\omega)\underline{I}(\omega)$

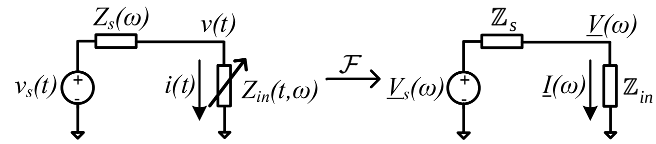

Figure 1. A general LPTV circuit with a time-varying load input impedance, and its conversion matrix equivalent circuit

by using the fact that the output of a sampled-output LPTV system is equivalent to that of an LTI system. The impulse response of the equivalent LTI system is easily obtained using the adjoint LPTV network [16], [17]. Nevertheless, it must be noted that considerable algebra is involved in each of these prior analysis. Further, certain circuit non-idealities such as non-ideal clock transitions, clock overlaps, etc. cannot be handled easily. Moreover, changes in the circuit topology (for example, due to parasitics) usually require a fresh analysis.

Conversion matrices have been recently proposed as a general method to analyze LPTV circuits [18]-[20]. It starts by expressing (1) as a matrix-vector equation. Assuming that the signals in the system are band-limited to $\left(-\left(K+\frac{1}{2}\right)\omega_p, \left(K+\frac{1}{2}\right)\omega_p\right]$ (K being a sufficiently large positive integer), define the frequency vector of the Fourier transform of any signal, $x(t)$, as the vector $\underline{X}(\omega) = \left[\begin{array}{cccc} X(\omega-K\omega_p) & X(\omega-(K-1)\omega_p) & \cdots & X(\omega+K\omega_p)\end{array}\right]^T$, $\omega\epsilon\left(-\frac{1}{2}\omega_p, \frac{1}{2}\omega_p\right]$, $X(\omega)$ being the Fourier transform of $x(t)$. Then it can be shown that the frequency vectors of the input and output, $\underline{U}(\omega)$ and $\underline{Y}(\omega)$ respectively, can be related using (1) by the expression $\underline{Y}(\omega) = \mathbb{H}(\omega)\underline{U}(\omega)$, where

$$\mathbb{H}(\omega) = \begin{bmatrix} H_{-K,-K}(\omega) & \cdots & H_{-K,0}(\omega) & \cdots & H_{-K,K}(\omega) \\ \vdots & \ddots & \vdots & \iddots & \vdots \\ H_{0,-K}(\omega) & \cdots & H_{0,0}(\omega) & \cdots & H_{0,K}(\omega) \\ \vdots & \iddots & \vdots & \ddots & \vdots \\ H_{K,-K}(\omega) & \cdots & H_{K,0}(\omega) & \cdots & H_{K,K}(\omega) \end{bmatrix} \quad (2)$$

is called the conversion matrix of the system [18]. Any element, $H_{i,j}(\omega)$, of $\mathbb{H}(\omega)$, is the transfer function from $U(\omega-j\omega_p)$ to $Y(\omega-i\omega_p)$, i.e. $H_{i,j}(\omega) = H_{i-j}(\omega+i\omega_p)$ (from (1)). It should be noted that the harmonic balance analysis of periodically time-varying circuits also treat inputs and outputs similarly as the formulation in (2), wherein the inputs and outputs are frequency-limited till a specified harmonic [21]. The phasor components at each frequency are then related together using the underlying circuit differential equations, and then solved using iterative methods such as those based on Kyrlov subspaces [22].

By itself, (2) is simply a different representation of (1). The difference is that for basic LPTV circuit elements, the relations between the frequency vectors of their voltages and currents is like LTI circuit elements as shown in Table I [20]. For example, in case of an LPTV resistor, $R(t) = R(t+T_p)$, the voltage-current relation $V(t) = R(t)i(t)$ can be expressed using the frequency vectors of the voltage and current, $\underline{V}(\omega)$ and $\underline{I}(\omega)$, respectively as $\underline{V}(\omega) = \mathbb{R}\underline{I}(\omega)$, where

$$\mathbb{R} = \begin{bmatrix} R_0 & R_{-1} & R_{-2} & \cdots & R_{-2K} \\ R_1 & \ddots & \ddots & \ddots & \vdots \\ R_2 & \ddots & R_0 & \ddots & R_{-2} \\ \vdots & \ddots & \ddots & \ddots & R_{-1} \\ R_{2K} & \cdots & R_2 & R_1 & R_0 \end{bmatrix} \quad (3)$$

is a frequency-independent Hermitian Toeplitz matrix whose components are obtained from the Fourier series expansion, $R(t) = \sum_{n=-\infty}^{\infty} R_n e^{jn\omega_p t}$. Note that a time-invariant resistor, $R(t) = R$ is represented simply by an identity matrix scaled by R. Similarly, LPTV capacitors and inductors are represented by the matrices, $\mathbb{C}$ and $\mathbb{L}$, respectively with the frequency-dependence of their impedances included using the diagonal matrix, $\mathbf{\Omega}(\omega) = diag\left\{\left[\omega - K\omega_p \quad \cdots \quad \omega \quad \cdots \quad \omega + K\omega_p\right]\right\}$. Also, the voltage and current frequency vectors follow basic circuit laws, such as Kirchhoff's laws. Thus, the conversion matrices of larger LPTV circuits can be derived by constructing their frequency-domain equivalent circuits (based on voltage and current frequency vectors, and the conversion matrices of the circuit elements), and then applying circuit laws. For example, the switches of a passive mixer or an N-path RF front-end can be modeled as resistors whose value toggles between appropriate R_{on} and R_{off} in a periodic manner [19], [20]. Such a representation is easily able to handle non-zero clock transition times [19] and clock-overlaps [20]. Further, small changes in circuit topology are also easily incorporated. Thus, the conversion matrix method provides a general and intuitive way of analyzing complex LPTV circuits.

This paper uses the conversion matrix analysis methodology to the problem of deriving the S_{11} of a general LPTV circuit. The result organically reveals effects such as reflections to harmonic shifts from input frequencies due to frequency translation. The analysis yields expressions to calculate the fraction of incident power reflected to input and other frequencies that is then applied to example LPTV receiver front-ends: (1) mixer-first receivers, (2) switched-capacitor receivers with reset, and (3) Filtering-by-Aliasing (FA)-based receiver front-ends. Explicit analytical expressions are derived for ideal N-path mixer-first receivers and FA-based receivers, while numerical results are obtained in other cases. The results are shown to match with simulated/measured results as well as with more narrow prior analysis.

II. S_{11} IN AN LPTV CIRCUIT

Consider an LPTV circuit shown in Fig. 1 where the source $V_s(t)$ with impedance $Z_s(\omega)$ is terminated in the circuit with a periodically time-varying load input impedance, $Z_{in}(t,\omega) = Z_{in}(t+T_p,\omega)$. To analyze this circuit, note the frequency-domain equivalent circuit shown in Fig. 1. The source and input impedances are represented by their conversion matrix equivalents, $\mathbb{Z}_s(\omega)$ and $\mathbb{Z}_{in}(\omega)$, respectively, with $\mathbb{Z}_s(\omega)$ being a diagonal matrix due to its time-invariant nature (the source impedance is usually a frequency-independent resistor, R_s, in which case $\mathbb{Z}_s(\omega) = R_s\mathbb{I}$, $\mathbb{I}$ being the identity matrix). The frequency-vectors of the voltage, $v(t)$, and current, $i(t)$, across the load are:

$$\begin{aligned} \underline{V}(\omega) = &\quad \mathbb{Z}_{in}(\omega)\left[\mathbb{Z}_s(\omega)+\mathbb{Z}_{in}(\omega)\right]^{-1}\underline{V_s}(\omega) \\ \underline{I}(\omega) = &\quad \left[\mathbb{Z}_s(\omega)+\mathbb{Z}_{in}(\omega)\right]^{-1}\underline{V_s}(\omega). \end{aligned} \tag{4}$$

By convention, the voltage and current delivered across the load can be represented by:

$$\begin{aligned} v(t) = &\quad v_I(t)+v_R(t), \\ i(t) = &\quad i_I(t)-i_R(t), \end{aligned} \tag{5}$$

where $v_I(t)$ and $v_R(t)$ are the incident and reflected voltages, respectively, while $i_I(t)$ and $i_R(t)$ are the incident and reflected currents, respectively. Further, the Fourier transforms of the incident waveforms, $v_I(t)$ and $i_I(t)$, are related by the relation $V_I(\omega) = Z_s(\omega)I_I(\omega)$, and similarly $V_R(\omega) = Z_s(\omega)I_R(\omega)$ for the reflected waveforms. Thus, the relations in (5) can be written in terms of the frequency-vectors of the incident and reflected voltages as

$$\begin{aligned} \underline{V}(\omega) = &\quad \underline{V_I}(\omega)+\underline{V_R}(\omega), \\ \underline{I}(\omega) = &\quad \mathbb{Z}_s^{-1}(\omega)\left[\underline{V_I}(\omega)-\underline{V_R}(\omega)\right]. \end{aligned} \tag{6}$$

Relating $\underline{V_I}(\omega)$ and $\underline{V_R}(\omega)$ by the familiar looking expression $\underline{V_R}(\omega) = \mathbb{S}_{11}(\omega)\underline{V_I}(\omega)$, and substituting (4) in (6) gives:

$$\mathbb{S}_{11}(\omega) = \left[\mathbb{Z}_{in}(\omega)-\mathbb{Z}_s(\omega)\right]\left[\mathbb{Z}_{in}(\omega)+\mathbb{Z}_s(\omega)\right]^{-1}. \tag{7}$$

The matrix $\mathbb{S}_{11}(\omega)$ relates the frequency vector of the reflected wave to the incident wave. Hence it can be said to be the conversion matrix corresponding to the "*LPTV reflection coefficient*". Equivalently, $\mathbb{S}_{11}(\omega)$ can also be expressed in terms of the source and load admittance conversion matrices, $\mathbb{Y}_s(\omega) = \mathbb{Z}_s^{-1}(\omega)$ and $\mathbb{Y}_{in}(\omega) = \mathbb{Z}_{in}^{-1}(\omega)$, respectively as

$$\mathbb{S}_{11}(\omega) = \mathbb{Y}_s^{-1}(\omega)\left[\mathbb{Y}_s(\omega)-\mathbb{Y}_{in}(\omega)\right]\left[\mathbb{Y}_s(\omega)+\mathbb{Y}_{in}(\omega)\right]^{-1}\mathbb{Y}_s(\omega). \tag{8}$$

Note that when $Z_s(\omega)$ is only resistive, $\mathbb{S}_{11}(\omega) = \left[\mathbb{Y}_s(\omega)-\mathbb{Y}_{in}(\omega)\right]\left[\mathbb{Y}_s(\omega)+\mathbb{Y}_{in}(\omega)\right]^{-1}$.

$\mathbb{S}_{11}(\omega)$ can be expressed in the general conversion matrix form from (2):

$$\mathbb{S}_{11}(\omega) = \begin{bmatrix} \gamma_{-K,-K}(\omega) & \cdots & \gamma_{-K,0}(\omega) & \cdots & \gamma_{-K,K}(\omega) \\ \vdots & \ddots & \vdots & \iddots & \vdots \\ \gamma_{0,-K}(\omega) & \cdots & \gamma_{0,0}(\omega) & \cdots & \gamma_{0,K}(\omega) \\ \vdots & \iddots & \vdots & \ddots & \vdots \\ \gamma_{K,-K}(\omega) & \cdots & \gamma_{K,0}(\omega) & \cdots & \gamma_{K,K}(\omega) \end{bmatrix} \tag{9}$$

Each element $\gamma_{i,j}(\omega)$ in $\mathbb{S}_{11}(\omega)$ relates the reflected wave generated at a frequency of $(i\omega_p+\omega)$ due to an incident wave at a frequency of $(j\omega_p+\omega)$, ω_p being the fundamental frequency of the system. In an LTI system, $\gamma_{i,j}(\omega) = 0\ \forall\, i \neq j$ because there is no frequency translation possible. Hence, $\mathbb{S}_{11}(\omega)$ is diagonal (expected since $\mathbb{Z}_{in}(\omega)$ is diagonal in LTI systems). In an LPTV circuit this is not true in general, implying that an incident wave can potentially create reflections at both its own frequency, as well as around harmonics of the fundamental frequency, ω_p.

Consider an LPTV circuit with an incident wave at a frequency, $(L\omega_p+\omega)$. Then the components of the reflected wave can be found using the $(L+K+1)^{th}$ column of $\mathbb{S}_{11}(\omega)$:

1) *Untranslated reflection*: The diagonal entry, $\gamma_{L,L}(\omega)$, represents the fraction of the incident voltage at frequency, $(L\omega_p+\omega)$, reflected at the same frequency. Thus, $\gamma_{L,L}(\omega)$ represents the LTI definition of S_{11}, i.e. $S_{11}(L\omega_p+\omega) = \gamma_{L,L}(\omega)$. Hence the fraction of incident power that is reflected untranslated in frequency is $|\gamma_{L,L}(\omega)|^2$.
2) *Harmonically translated reflections:* The non-diagonal entries, $\{\gamma_{i,L}(\omega)\}_{i\neq L}$, represents the fraction of the incident voltage reflected to frequencies that are offset by harmonics of ω_p compared to the incident frequency, $(L\omega_p+\omega)$. Hence the total fraction of incident power reflected to harmonic frequency offsets is given by $\sum\limits_{i\neq L}|\gamma_{i,L}(\omega)|^2$ (sum of the reflected power at each harmonic).

In most LPTV receiver front-ends, such as N-path filters and mixer-first receivers, the fundamental frequency, ω_p, is the same as the receiver LO frequency. Hence, the in-band incident signal is expected to be around frequencies of $\pm\omega_p$. Thus for computing reflections (or antenna reradiation), the components of interest in $\mathbb{S}_{11}(\omega)$ are $\{\gamma_{i,1}(\omega)\}$ and $\{\gamma_{i,-1}(\omega)\}$. For example, the total fraction of the in-band incident power at a frequency, $(\omega_p+\omega)$, reflected to the antenna is given by $\sum\limits_i|\gamma_{i,1}(\omega)|^2$, with $|\gamma_{1,1}(\omega)|^2$ being the fraction of in-band reflected power.

Thus, forming the $\mathbb{S}_{11}(\omega)$ matrix from (7)-(9) is enough to calculate the S_{11} and reflections in the LPTV system. Nevertheless, a large enough K needs be chosen to get accurate results, with convergence to the true solution as $K\to\infty$. For certain special cases, an analytical solution can be derived using properties of series of matrices.

The application of this approach is next illustrated with a simple example. Subsequent sections will apply it to typical LPTV receiver front ends.

A Simple Example

Consider the case when both the source and load are memoryless, i.e., $Z_s(\omega) = R_s$ and $Z_{in}(t,\omega) = R_{in}(t)$. Denoting the conversion matrix of $R_{in}(t)$ by $\mathbb{R}_{in}$, (7) gives

$$\mathbb{S}_{11}(\omega) = \left[\mathbb{R}_{in}-R_s\mathbb{I}\right]\left[\mathbb{R}_{in}+R_s\mathbb{I}\right]^{-1}. \tag{10}$$

Let $\mathbb{X}_K = \mathbb{R}_{in}+R_s\mathbb{I}$, and $\mathbb{W}_K = \mathbb{R}_{in}-R_s\mathbb{I}$ denote two $(2K+1)\times(2K+1)$ matrices. Consider the sequence of matrices, $\{\mathbb{X}_K\}$ and $\{\mathbb{W}_K\}$. Each matrix in the sequences, $\mathbb{X}_K$

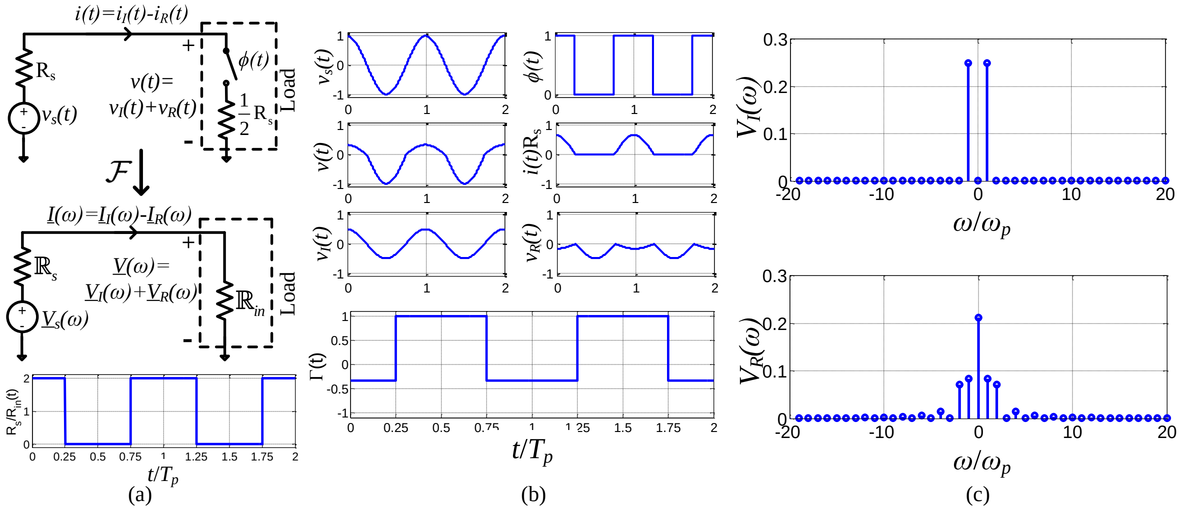

Figure 2. (a) A simple LPTV circuit with a memoryless load impedance, (b) time-domain waveforms for an input of $v_s(t) = cos(\omega_p t)$, and (c) magnitude of the Fourier transforms of the incident and reflected voltage waveforms

and $\mathbb{W}_K$, are Hermitian Toeplitz whose elements can be shown to be the Fourier series coefficients of the periodic functions, $x(t) = R_{in}(t)+R_s > 0$ and $w(t) = R_{in}(t)-R_s$, respectively. By using Lemma 4.5 in [23], it can be shown that the sequence of inverse matrices, $\{\mathbb{X}_K^{-1}\}$, will converge[1] to a Circulant[2] matrix whose elements are the Fourier series coefficients of $1/x(t)$ as $K \to \infty$. Further, $\{\mathbb{W}_K\mathbb{X}_K^{-1}\}$ will also converge to a Circulant matrix whose elements are the Fourier series coefficients of $w(t)/x(t) = [R_{in}(t) - R_s] / [R_{in}(t) + R_s]$. Thus, using the equivalence[3] of convergent series of Toeplitz and Circulant matrices, $\mathbb{S}_{11}(\omega)$ in (9) will be a Hermitian Toeplitz matrix whose elements are the Fourier series coefficients of $\Gamma(t) \triangleq [R_{in}(t) - R_s] / [R_{in}(t) + R_s]$. Note that $\Gamma(t)$ is periodic with the same period as $R_{in}(t)$. Specifically, if $\Gamma(t) = \sum_{n=-\infty}^{\infty} \gamma_n e^{jn\omega_p t}$, $\mathbb{S}_{11}(\omega)$ is given by

$$\mathbb{S}_{11} = \begin{bmatrix} \gamma_0 & \gamma_{-1} & \gamma_{-2} & \cdots & \gamma_{-2K} \\ \gamma_1 & \ddots & \ddots & \ddots & \vdots \\ \gamma_2 & \ddots & \gamma_0 & \ddots & \gamma_{-2} \\ \vdots & \ddots & \ddots & \ddots & \gamma_{-1} \\ \gamma_{2K} & \cdots & \gamma_2 & \gamma_1 & \gamma_0 \end{bmatrix}, \quad (11)$$

i.e. $\mathbb{S}_{11}$ is a Hermitian Toeplitz matrix whose elements are the Fourier series coefficients of $\Gamma(t)$. This makes intuitive sense since given the memoryless source and load impedances of R_s and $R_{in}(t)$, respectively, the instantaneous reflected and incident voltages are simply related as $v_R(t) = \Gamma(t)v_I(t)$.

Consider the simple circuit shown in Fig. 2(a) to illustrate the usefulness of this analysis. The load consists of a resistance of $R_s/2$ in series with a switch controlled by a 50% duty cycle clock, $\phi(t)$, with period, T_p. Note that the average conductance of the load is $1/R_s$, i.e. it presents an impedance of R_s when driven by an ideal voltage source. However, when driven by a source with resistance, R_s, the reflected wave is non-zero (seen in the time-domain waveforms in Fig. 2(b)), and so it is not impedance matched (alternatively, if the load were the switch in parallel with a resistance of $2R_s$, the impedance presented to an ideal current source would be R_s, but the reflected wave will still be non-zero). Further, for a sinusoidal input at frequency, $\omega_p = 2\pi/T_p$, both the voltage and current across the load have components at frequencies other than $\pm\omega_p$. Thus, the S_{11} and reflections are non-zero even though the input impedance/admittance might equal the source impedance for a particular case (for example, ideal voltage source). This is a reflection of the fact that the input impedance in LPTV circuits is actually source-dependent, and changes with source impedance [4], [15].

The circuit shown in Fig. 2(a) is memoryless. Hence its $\mathbb{S}_{11}(\omega)$ matrix is simply given by (11) that can be calculated from the reflection coefficient, $\Gamma(t)$. It can be easily seen that

$$\Gamma(t) = \begin{cases} 1 & \phi(t) = 0 \\ -1/3 & \phi(t) = 1, \end{cases}$$

and so $\gamma_n = -\frac{2}{3} sinc\left(\frac{n\pi}{2}\right)$ [4] for $n \neq 0$, and $\gamma_0 = \frac{1}{3}$. Note that the diagonal elements, γ_0, that give the S_{11} are non-zero. Using (5) it can also be shown that $v_I(t) = v_s(t)/2$, i.e. the incident wave is half the source voltage (always true when the source resistance is resistive and is the reference resistor for S-parameters). Since $v_s(t) = cos(\omega_p t)$, the frequency vector, $\underline{V_I}(\omega = 0)$ is simply $\begin{bmatrix} \cdots & 0 & \frac{1}{4} & 0 & \frac{1}{4} & 0 & \cdots \end{bmatrix}^T$. Hence the reflected wave is simply given by $\underline{V_R}(\omega = 0) = \mathbb{S}_{11}\underline{V_I}(\omega = 0)$

[1]Strictly speaking, the convergence is true for any absolute-summable $x(t)$. While ideal square wave clocks may violate this condition, in reality the rise/fall times are non-zero, and so absolute summability is maintained.

[2]A special kind of Toeplitz matrix where each row vector is rotated one element to the right relative to the preceding row vector.

[3]The equivalence means that the conversion matrices for basic elements can also be expressed as Circulant matrices, with results converging as $K \to \infty$.

[4]This paper uses the unnormalized $sinc$ function, i.e. $sinc(x) = sin(x)/x$.

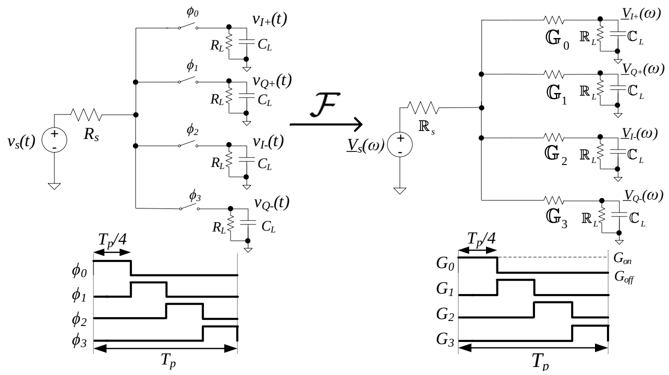

Figure 3. A simple 4-path mixer-first receiver front-end

$$= \frac{1}{12\pi}\begin{bmatrix} \pi & -4 & 0 & \cdots & \\ -4 & \ddots & \ddots & \ddots & \vdots \\ 0 & \ddots & \pi & \ddots & 0 \\ \vdots & \ddots & \ddots & \ddots & -4 \\ & \cdots & 0 & -4 & \pi \end{bmatrix}\begin{bmatrix} \vdots \\ 1 \\ 0 \\ 1 \\ \vdots \end{bmatrix} = \frac{1}{12\pi}\begin{bmatrix} \vdots \\ \pi \\ -8 \\ \pi \\ \vdots \end{bmatrix}.$$

Note that $\underline{V_I}(\omega \neq 0) = \underline{V_R}(\omega \neq 0) = \begin{bmatrix} \cdots & 0 & \cdots \end{bmatrix}^T$ since the input is only at ω_p. The calculation clearly shows that a component exists in the DC band in $\underline{V_R}(\omega)$ that is absent in $\underline{V_I}(\omega)$, thus revealing reflections to harmonic offset frequencies. The calculated Fourier transforms of the incident and reflected voltage signals are shown in Fig. 2(c), and are consistent with the time-domain waveforms in Fig. 2(b). Thus, the conversion matrix technique easily predicts the S_{11} and reflections in this example LPTV circuit.

The conversion matrix technique can similarly be applied to other LPTV circuits as well. Specifically, similar analysis can now be used to discuss impedance matching in some typical LPTV receiver front-ends. As mentioned before, in some cases, closed form analytical expressions are possible whereas in other cases, the $\mathbb{S}_{11}(\omega)$ matrix can be numerically evaluated (e.g., using MATLAB) for a sufficiently large K.

III. Mixer-First Receivers

Mixer-first receivers (such as the 4-path receiver shown in Fig. 3) are promising candidates for widely programmable RF receiver front-ends. The RF input signal is downconverted by a set of N passive mixer switches controlled by clocks with duty cycle, $1/N$, and period, T_p, as shown in the figure. This equivalently results in the baseband low pass filter response being upconverted to give a high-Q band pass filter centered at the clock frequency, $\omega_p = 2\pi/T_p$ (and its harmonics). Adding a parallel resistance to the baseband capacitor can be shown to allow RF impedance matching as well.

Consider the frequency-domain equivalent circuit of the 4-path mixer shown in Fig. 3, reproduced from [19]. The input impedance matrix of the circuit is given by [19]

$$\mathbb{Z}_{in}(\omega) = \mathbb{Y}_{in}^{-1}(\omega) = \left(\sum_{n=0}^{3}\left[\mathbb{Z}_L + \mathbb{G}_n^{-1}\right]^{-1}\right)^{-1}, \quad (12)$$

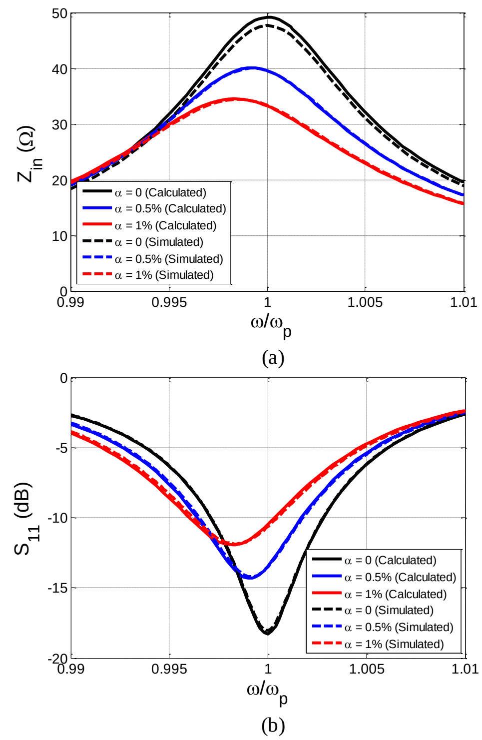

Figure 4. (a) Input impedance presented to an ideal current source, and (b) S_{11} around the LO frequency in a 4-path mixer-first receiver with the presence of parasitic capacitance, $C_p = \alpha C_L$, at the antenna input when $R_L = \frac{\pi^2}{2}R_s$

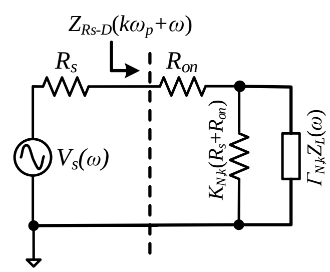

Figure 5. Equivalent LTI circuit of an N-path mixer-first receiver around the frequency, $k\omega_p$

where $\mathbb{G}_n$ is the conversion matrix of the switch conductance in path n (a Hermitian Toeplitz matrix derived from the conductance waveform, $G_n(t)$ shown in Fig. 3), and $\mathbb{Z}_L(\omega) = \left[R_L^{-1}\mathbb{I} + jC_L\mathbf{\Omega}(\omega)\right]^{-1}$ is the LTI path load impedance. Then using (7), $\mathbb{S}_{11}(\omega)$ can be easily calculated. The analysis can also easily include circuit imperfections. For example, the impedance is disturbed by the presence of parasitic capacitance at the antenna (from, for example, the mixer switches). This is because the switches must be made large to reduce its ON resistance that directly limits the out-of-band rejection of the realized band-pass filter [2]. Hence consider a capacitance, $C_p = \alpha C_L$ at the input of the receiver, and its corresponding admittance conversion matrix, $\mathbb{Y}_p(\omega) = jC_p\mathbf{\Omega}(\omega)$. Then the input impedance can be simply modified to

$$\mathbb{Z}_{in}^{'}(\omega) = \left(\mathbb{Y}_p(\omega) + \mathbb{Y}_{in}(\omega)\right)^{-1}, \quad (13)$$

while $\mathbb{S}_{11}(\omega)$ retains the expression in (7) [19].

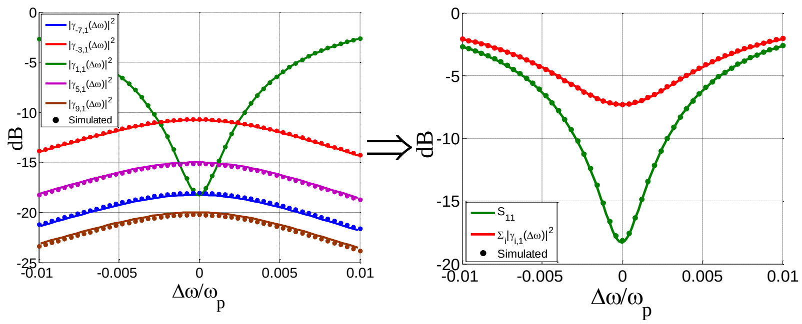

Figure 6. Calculated fraction of input power reflected to LO harmonics, and the total fraction of power reflected for an incident signal around LO frequency, ω_p, in a 4-path mixer-first receiver for $R_L = \frac{\pi^2}{2} R_s$

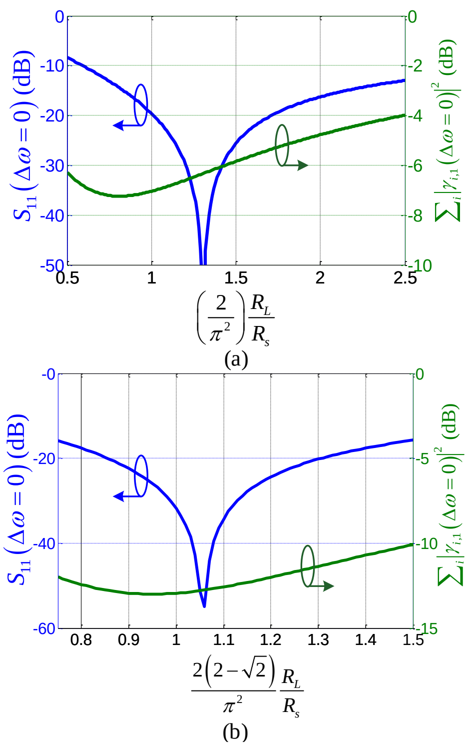

Figure 7. $S_{11}$and total reflected power for an incident signal at the receiver center frequency, ω_p, as a function of baseband resistance, R_L, in (a) a 4-path, and (b) an 8-path mixer-first receiver

To illustrate the results obtained from the analysis, consider the case when $R_L = \frac{1}{4} sinc^2\left(\frac{\pi}{4}\right) R_s = \frac{\pi^2}{2} R_s$. It is well known that if $1/R_L C_L \ll \omega_p$, then this ensures that the impedance presented by the receiver to an ideal current source at $\omega = \omega_p$ is R_s [9], [10] (due to impedance translational property of current-driven passive mixers). Fig. 4 shows simulated and calculated results (with $K = 1000$)[5] for this case with $R_s = 50\Omega$, $R_{on} = 1/G_{on} = 0.1\Omega$, $G_{off} = 0$, and ω_p set to $50/R_s C_L$. It is seen that the input impedance presented to an ideal current is about 50Ω at the center frequency, ω_p (obtained from the $(K+2, K+2)^{th}$ term in $\mathbb{Z}_{in}(\omega)$). However, the calculated S_{11} (obtained from the $(K+2, K+2)^{th}$ term in $\mathbb{S}_{11}(\omega)$) is only -18dB (verified using Spectre RF PSS-PSP/PAC simulations), indicating that the impedance presented to the $R_s = 50\Omega$ source is no longer R_s. This is because just as in the simple example in Section II, the impedance presented changes with the source. [3]-[5] models it with a shunt element, R_{sh}, dependent on R_s appearing along with the upconverted baseband impedance. In any case, the effect of non-zero α, shown in [5], [17], is also replicated correctly by the analysis, with the impedance and S_{11} peaks shifting to lower frequencies.

[5] $K = 1000$ is sufficient for accurate results, with no noticeable difference in results with higher K. A short discussion on the size of matrices is included in Appendix B.

While the matrix equations from (12) and (7) can be solved numerically to obtain results like Fig. 4, it can also be simplified to derive closed-form expressions. Appendix A derives the input impedance and S_{11} for an ideal N-path mixer-first receiver. The analysis leads to closed-form expressions for all elements of the matrices, $\mathbb{Y}_{in}(\omega)$, $\mathbb{Z}_{in}(\omega)$ and $\mathbb{S}_{11}(\omega)$ given by (21), (23), and (25), respectively. Corresponding impedances are also found from diagonal elements, and agree with results in prior art (for example, impedance presented to an ideal current source, $Z_{C-D}(k\omega_p + \omega)$, given by (24) [9], [10], and to a source with impedance R_s, $Z_{Rs-D}(k\omega_p + \omega)$, given by (26) [3]-[5]). In fact, $Z_{Rs-D}(k\omega_p + \omega)$ can be shown to have an equivalent circuit shown in Fig. 5, where

$$K_{N,k} = \frac{sinc^2\left(\frac{k\pi}{N}\right)}{1 - sinc^2\left(\frac{k\pi}{N}\right)},\ \Gamma_{N,k} = \frac{1}{N} sinc^2\left(\frac{k\pi}{N}\right).$$

This equivalent circuit matches the LTI equivalent circuit derived for $k = 1$ in prior art [3]-[5]. Further, for $R_{on} = 0\Omega$, $S_{11}(k\omega_p) = 0$ can be obtained (using (26)) with

$$R_L = \frac{N R_s}{2 sinc^2\left(\frac{k\pi}{N}\right) - 1}. \tag{14}$$

Note that $R_L < 0$ when impedance match is not possible (cases where $K_{N,k} < 1$ results in $Z_{Rs-D}(k\omega_p) < R_s$).

While the in-band S_{11} can ideally be reduced to 0, the total reflected power must be considered as well. The non-diagonal terms of the matrix, $\mathbb{S}_{11}(\omega)$, obtained in (25) must be considered as described in Section II. Figure 6 shows the calculated fraction of power reflected for an in-band input incident signal in an ideal 4-path receiver for $R_{on} = 0\Omega$ and $R_L = \frac{\pi^2}{2} R_s$ for fundamental operation, i.e. $k = 1$. $|\gamma_{i,1}(\Delta\omega)|^2$ is the fraction of the incident power reflected to the frequency, $(i\omega_p + \Delta\omega)$ when the incident wave is at the frequency, $(\omega_p + \Delta\omega)$. As

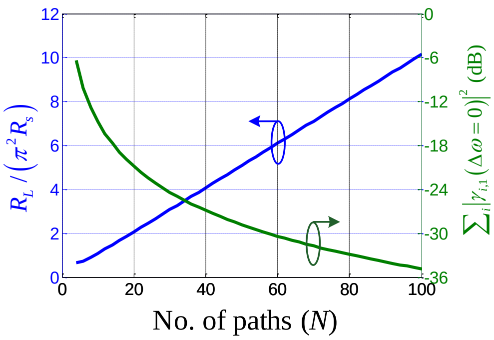

Figure 8. Variation of baseband resistance, R_L, needed for $S_{11} \approx 0$ and total reflected power for an incident signal at receiver center frequency, ω_p, with no. of paths, N, in a mixer-first receiver

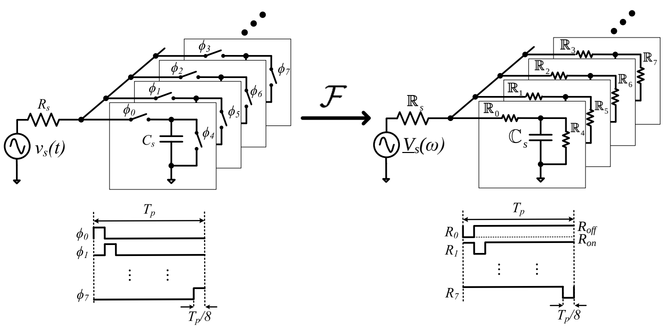

Figure 9. A simple 8-path receiver front-end with switched-capacitors for impedance matching

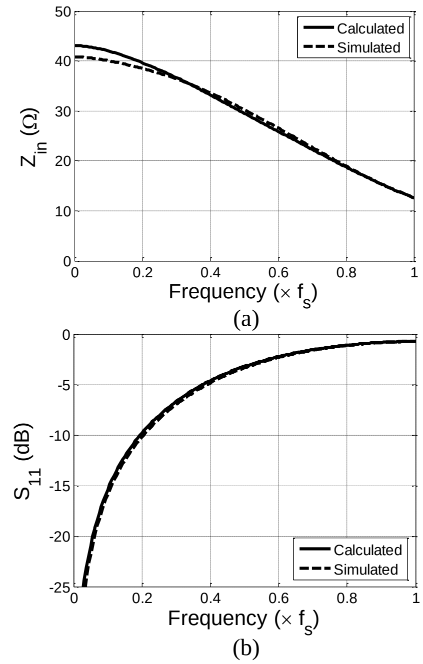

Figure 10. (a) Input impedance presented to an ideal current source, and (b) wideband S_{11} of the 8-path switched-capacitor receiver front-end with switch $R_{on} = 0.5\Omega$

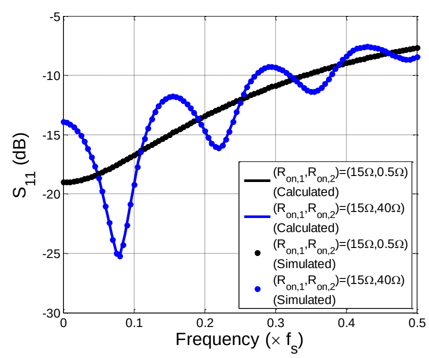

Figure 11. Effect of switch resistances on S_{11} of the switched-capacitor receiver front-end with input and reset switch resistances of $R_{on,1}$ and $R_{on,2}$, respectively

derived in Appendix A, an N-path structure causes reflections to only frequency offsets of $N\omega_p$ and its multiples, and so in the 4-path case, $\gamma_{1,1+n}(\Delta\omega) = 0\,\forall\, n \neq 4m,\, m \,\epsilon\, \mathbb{Z}$. The total fraction of reflected power is also plotted (along with $S_{11} = |\gamma_{1,1}(\Delta\omega)|^2$ for comparison). It can be seen that for an incident wave at the LO frequency, about -7.3dB (or 19%) of the total incident power is reflected. This is a significant amount, and is about 10dB worse than the in-band reflected power inferred from S_{11} alone. Thus, reflections to non-input frequencies need to be considered when employing impedance matching with the structure in Fig. 3.

It is desirable to minimize the total reflected power. Varying R_L (while keeping $R_L C_L$ constant) changes S_{11} and total reflected power for fundamental operation as shown in Fig. 7(a). While S_{11} is 0 when $R_L \approx 6.44 R_s$ (as expected from (14)), the total reflected power is still close to minimum when R_L is set to $\frac{\pi^2}{2} R_s$. Nevertheless, the difference is small (<1dB). Another alternative is to increase the number of paths, N. For example, an 8-path receiver eliminates reflections from frequency offsets of $4\omega_p$ and its odd multiples compared to a 4-path receiver. As shown in Fig. 7(b), this significantly improves the total fraction of reflected power to less than -13dB. S_{11} is 0 at the expected $R_L \approx 8.9 R_s$, but total reflection is slightly lower when R_L is set to present an impedance of R_s to a current source, i.e. $R_L = \frac{1}{8} sinc^2\left(\frac{\pi}{8}\right) R_s = \pi^2 / \left[2\left(2-\sqrt{2}\right)\right] R_s$.

The total reflected power can be derived as a function of the no. of paths, N, as well. Substituting the optimal value of R_L needed for impedance match at $k\omega_p$, i.e., $S_{11}(k\omega_p) = 0$ (from (14)) in (25) (along with $R_{on} = 0\Omega$) gives

$$\sum_{i=-\infty}^{\infty} |\gamma_{i,k}(\Delta\omega = 0)|^2 = \frac{1 - sinc^2\left(\frac{k\pi}{N}\right)}{sinc^2\left(\frac{k\pi}{N}\right)} = \frac{1}{K_{N,k}}. \qquad (15)$$

Note that the total reflected power worsens for non-fundamental operation, i.e. $|k| > 1$ (optimal R_L varies with k as per (14)). Figure 8 shows the variation of the optimal R_L and total reflected power as a function of N for $k = 1$. The fraction of power reflected clearly reduces by ~6dB for every doubling of N, while R_L grows linearly with N.

IV. Switched-Capacitor Receiver With Reset

An alternative method to achieve impedance matching is using switched-capacitors that are reset periodically [13]. By charging and discharging load capacitors, C_s, in N paths, where each path is turned on for $1/N^{th}$ of the LO period,

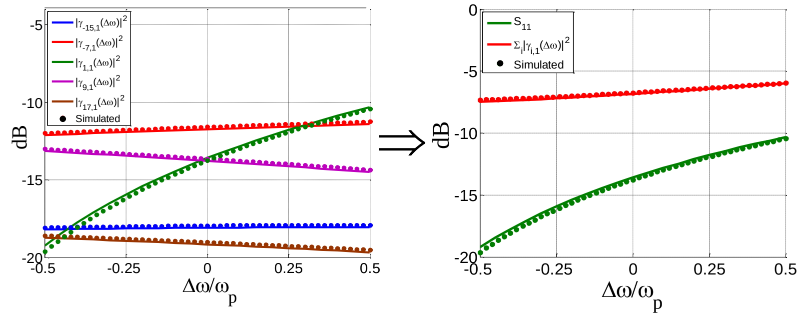

Figure 12. Calculated fraction of input power reflected to LO harmonics, and the total fraction of power reflected (considering the fundamental and up to 50 harmonics) for an incident wave around the receiver center frequency, $\omega_p = 2\pi(f_s/8)$, in an 8-path switched-capacitor receiver front-end

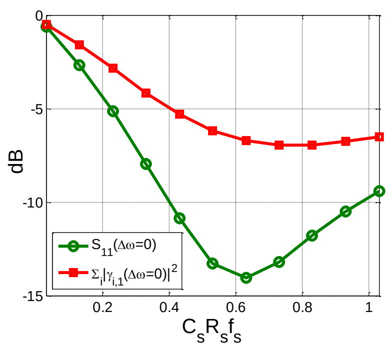

Figure 13. S_{11} and total reflected power (considering up to 50 harmonics) for an incident wave at the receiver center frequency, $\omega_p = 2\pi(f_s/8)$, as a function of capacitance, C_s, in an 8-path switched-capacitor receiver front-end

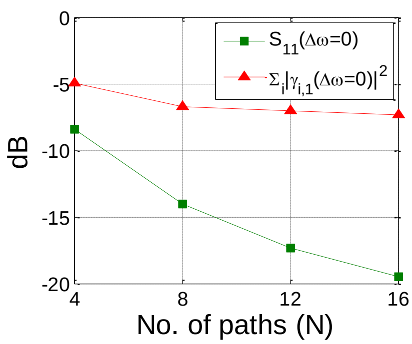

Figure 14. Variation of S_{11} and total reflected power (considering up to 50 harmonics) for an incident wave at the receiver center frequency, $\omega_p = 2\pi(f_s/N)$, as a function of no. of paths, N, in the switched-capacitor receiver front-end

T_p, a switched-capacitor resistance is achieved at the input that can be matched to the source impedance, R_s. Figure 9 shows an 8-path example that was implemented in [13]. It was shown that a wideband match is achieved in this circuit for $C_s \approx 0.63/(f_s R_s)$, where $f_s = 8/T_p$. From the frequency-domain conversion matrix equivalent circuit shown in Fig. 9, the input impedance of the circuit can be derived using series and parallel combination of impedances as

$$\mathbb{Z}_{in}(\omega) = \left(\sum_{i=0}^{N-1} \left[\left\{ \mathbb{Y}_L(\omega) + \mathbb{R}_j^{-1} \right\}^{-1} + \mathbb{R}_i \right]^{-1} \right)^{-1}, \quad (16)$$

where $\mathbb{R}_i$ and $\mathbb{R}_j$ are the conversion matrices of the i^{th} path's input-switch and the reset-switch resistances respectively with $j = (i + N/2) \bmod N$, and $\mathbb{Y}_L(\omega) = jC_s\mathbf{\Omega}(\omega)$ is the admittance of the load capacitor, C_s (Note the summation in (16) can be expressed as a function of only one path using the $\mathbb{P}_N$ matrix (like the mixer-first receiver in Appendix A)). Then using (7), $\mathbb{S}_{11}(\omega)$ is easily calculated. Figure 10 shows the calculated input impedance (presented to an ideal current source), and S_{11} of the circuit (for $K = 1000$) with $R_s = 50\Omega$, $R_{on} = 0.5\Omega$ and $R_{off} = 50k\Omega$ [6]. The results compare well with simulated results using Spectre RF and the results in [13]. The S_{11} is low in the wideband, and better than -25dB at DC. The S_{11} does degrade to -13dB at the LO frequency, $\omega_p = 2\pi/T_p$.

[6]Finite R_{off} is assumed to ensure that the matrix algebra is tractable.

Other effects are also easily included. For example, the ON-resistances of the input and reset switches, $R_{on,1}$ and $R_{on,2}$, respectively can be simply included while constructing the $\mathbb{R}_i$ and $\mathbb{R}_j$ matrices in (16). Figure 11 shows that calculated S_{11} for practical values of $R_{on,1}$ and $R_{on,2}$ as mentioned in [13]. The results match very well with results from Spectre RF simulations, as well as Fig. 5 in [13]. It is notable that calculated results were not available for all cases in [13].

Finally, the non-diagonal terms of the matrix, $\mathbb{S}_{11}(\omega)$, can be considered to characterize reflections to harmonic offsets from the input frequency. Figure 12 shows the calculated fraction of power reflected for an in-band input incident wave (with $R_{on,1} = R_{on,2} = 0.5\Omega$), where $|\gamma_{i,1}(\omega)|^2$ is the fraction of the incident power reflected to the frequency, $(i\omega_p + \Delta\omega)$ when the incident wave is at the frequency, $(\omega_p + \Delta\omega)$. As expected, significant reflections are present at frequency offsets of $8\omega_p$ and its multiples due to the 8-path receiver structure (similar to an 8-path mixer-first receiver). The total fraction of reflected power (for up to 50 LO harmonics) is also plotted (along with $S_{11} = |\gamma_{1,1}(\Delta\omega)|^2$ for comparison). It can be noted that the total fraction of reflected power is about -6.8dB, which is significantly worse than for an 8-path mixer-first receiver. Further, varying C_s from its impedance-matched value of $0.63/(f_s R_s)$ does not improve reflections as shown in Fig. 13. Finally, Fig. 14 plots the variation of S_{11} and total reflected power with no. of paths, N, in the receiver. While S_{11} does improve with N, the calculated total fraction of reflected

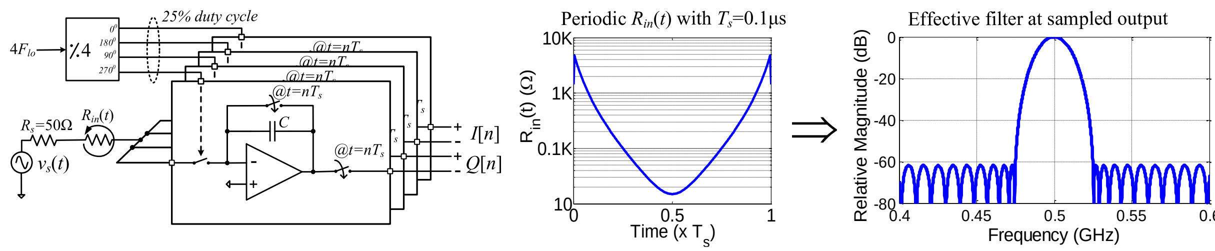

Figure 15. A simple Filtering-by-Aliasing (FA)-based receiver front-end

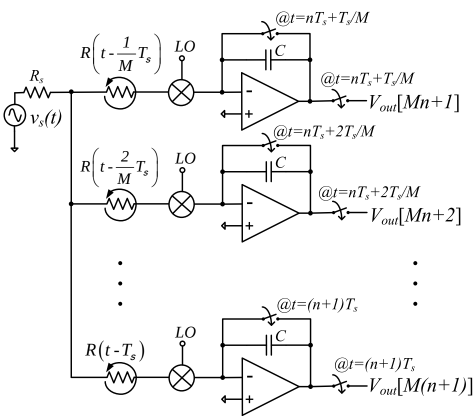

Figure 16. An M-way time-interleaved FA-based receiver front-end

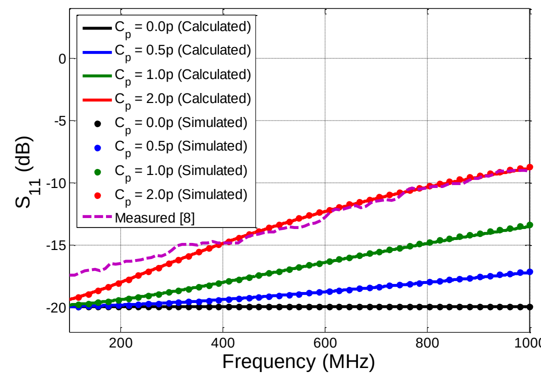

Figure 17. Wideband S_{11} of an FA-based receiver front-end with the presence of parasitic capacitance, C_p, at the antenna input, and comparison of the measured S_{11} in [8] to calculations

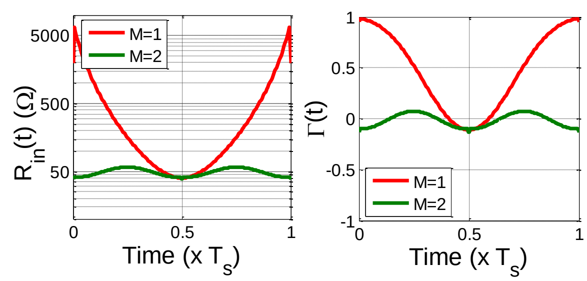

Figure 18. The time-varying input resistance, $R_{in}(t)$ and the corresponding $\Gamma(t)$ for non-interleaved and 2-way interleaved implementation of filter frequency response in Fig. 15 with min. LPTV resistor resistance, $R_{min} = 40\Omega$

power was -7.7dB even for a 16-path implementation. Hence, the switched-capacitor impedance matching structure may not ideal by itself when antenna reradiation must be minimized.

V. FA-Based Receiver Front-Ends

Recent works have used time-varying components to realize sharp programmable receiver front-ends [7], [8]. Based on the technique called Filtering by Aliasing (FA) [24], these receivers use LPTV resistors followed by integrators as shown in Fig. 15. When the integrators are operated as integrate-and-dump blocks, with the outputs sampled and reset at the same period, T_s, as the time-varying resistors, it was shown that sharp programmable analog-FIR filter responses of length T_s, controlled precisely by the resistance variation $R_{in}(t)$, were achieved from the input, $v_s(t)$, to the sampled baseband outputs (as shown in Fig. 15) [7]. A 4-path mixer was used to upconvert the filter to a desired center frequency.

The performance of FA-based receivers was further extended using the concept of time-interleaving. As shown in Fig. 16, M identical receiver front-ends are connected in parallel to the source, except that their sampling clocks and input resistance variations are phase-shifted in a time-interleaved manner. This allows the receiver to implement an analog-FIR filter whose length is M times the effective sampling period. For example, in Fig. 16 the sampling period T_s/M for a filter of length T_s. A 2-way interleaved front-end was implemented in [8] with improved filtering performance compared to [7].

The conversion matrix technique can be easily used to study impedance matching in the FA-based receiver front-ends. Assuming that the op-amp is ideal in Fig. 15, the input impedance is simply a time-varying resistance $R_{in}(t)$ (for a single-stage op-amp implementation like in [7], the integrator input impedance, $1/g_m$, needs to be added). Similarly, for the time-interleaved case, the input impedance, $R_{in}(t)$, is the parallel combination of the time-varying resistances in the M paths. For example, in case of a 2-way time-interleaved receiver [8], $R_{in}(t) = R(t)||R(t - T_s/2)$. Note that unlike previously discussed front-ends, the input impedance is ideally memoryless. Further, the periodicity of the impedance is at the baseband sampling rate, T_s, and not the receiver center frequency. Thus, the ideal input impedance is simply given by the conversion matrix of $R_{in}(t)$, i.e. $\mathbb{R}_{in}$, and so $\mathbb{S}_{11}(\omega)$ is simply given by

$$\mathbb{S}_{11}(\omega) = [\mathbb{R}_{in} - R_s\mathbb{I}]\,[\mathbb{R}_{in} + R_s\mathbb{I}]^{-1}, \tag{17}$$

where R_s is the source impedance. As discussed in Section

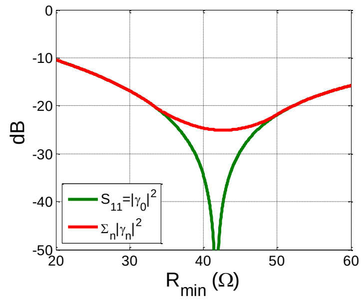

Figure 19. Variation of S_{11} and total reflected power with min. LPTV resistor resistance, R_{min} for 2-way time-interleaved implementation of filter in Fig. 15

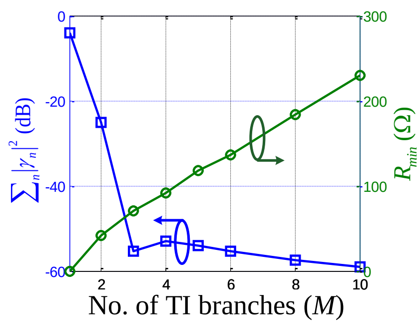

Figure 20. Variation of R_{min} and total reflected power with no. of time-interleaved branches, M

II, since the input impedance is memoryless, $\mathbb{S}_{11}(\omega)$ can be simply constructed from the Fourier series of time-varying reflection coefficient, $\Gamma(t)$, as shown in (11). Hence, the S_{11} of the circuit is simply given by the diagonal elements of $\mathbb{S}_{11}(\omega)$,

$$S_{11,ideal} = \gamma_0 = mean\left[\frac{R_{in}(t) - R_s}{R_{in}(t) + R_s}\right], \tag{18}$$

exactly as noted in [7]. The S_{11} is frequency-independent, and so can be kept low in the wideband.

Presence of parasitics can also be easily considered. For example, consider a parasitic capacitance, C_p at the input of the receiver. Then the input impedance expression changes to

$$\mathbb{Z}_{in}(\omega) = \left(\mathbb{Y}_p(\omega) + \mathbb{R}_{in}^{-1}\right)^{-1}, \tag{19}$$

where $\mathbb{Y}_p(\omega) = jC_p\mathbf{\Omega}(\omega)$ is the admittance conversion matrix of C_p. Hence the S_{11} becomes frequency dependent. Figure 17 shows the effect of C_p on the S_{11} of the receiver front-end when the resistance variation is designed to give a wideband $S_{11,ideal} = -20$dB (from [8]), calculated for $K = 1000$. As expected, the S_{11} is -20dB regardless of frequency for $C_p = 0$ from both calculations as well as Spectre RF PSS-PSP simulations. With the presence of C_p, the S_{11} degrades at higher frequencies. Further, comparison with the measured S_{11} in [8] with the estimated $C_p = 2$pF (see Fig. 17) shows that the calculations match well with prior results.

The total amount of reflected power to the antenna that is reradiated can also be easily calculated. With $C_p = 0$, the non-diagonal components of $\mathbb{S}_{11}(\omega)$ are simply the non-DC Fourier series coefficients of $\Gamma(t)$. Thus, for an in-band incident wave, the total fraction of power reflected can be found using Parseval's theorem to be

$$\sum_{n=-\infty}^{\infty} |\gamma_n|^2 = \frac{1}{T_s}\int_{t=0}^{T_s} |\Gamma(t)|^2\, dt = mean\left[|\Gamma(t)|^2\right].$$

This depends on the actual resistance variation, but as a trivial example, the mean can be set to 0 by setting $\Gamma(t) = 0$, i.e. $R_{in}(t) = R_s$. Of course, this would only result in a simple first-order baseband filter similar to the mixer-first receiver in [6].

The example resistance variation shown in Fig. 15 cannot achieve low S_{11} due to its large range of variation. Hence, the filter impulse responses were themselves optimized in [7], [8] to allow for low S_{11}. While the details of such an optimization can be found in [25], it can be shown that increasing the no. of time-interleaved branches, M, can lead to low S_{11} and reflections. Consider the case where the filter shown in Fig. 15 is designed with LPTV resistors that can achieve a minimum value of $R_{min} = 40\Omega$. As before, if no time-interleaving is applied, the input resistance variation, $R_{in}(t)$, is large and as shown $\Gamma(t)$ is > 0 for most of the period leading to a large S_{11}. Suppose, if 2-way time-interleaving is used. The resistance variation, $R(t)$, in each branch is still similar to the non-interleaved case. The input resistance, $R_{in}(t)$, on the other hand, is the parallel combination of $R(t)$ and $R(t - T_s/2)$. Thus, it remains fairly constant as shown in Fig. 18. The choice of $R_{min} = 40\Omega$ keeps it close to $R_s = 50\Omega$, i.e., $\Gamma(t) \approx 0$ throughout the period. Hence the 2-way interleaved implementation is much better in terms of S_{11} and reflections. Nevertheless, choosing the right value of R_{min} is critical. Figure 19 shows the variation of S_{11} and total reflected power for the 2-way time-interleaved implementation with R_{min}. The fraction of power reflected can be made as small as -25dB, and $S_{11} \approx 0$ by choosing $R_{min} \approx 42\Omega$ in this case. Further increasing the number of branches, M, reduces reflections to almost 0 (as shown in Fig. 20), with R_{min} scaling inversely with M as intuitively expected. In fact, just 3-way interleaving is sufficient to nearly eliminate all reflections. These trends hold true with other filter impulse responses as well.

VI. Conclusions

This paper introduced a conversion matrix-based analysis to understand impedance matching in general LPTV circuits. The analysis is used to easily derive the S_{11} in an LPTV circuit, and simultaneously predicts reflections to harmonic offsets from input frequencies. Application to example LPTV receiver front-ends provides new insights to reflections and possible reradiation from the antenna when connected to such circuits. Explicit expressions have been derived for both ideal N-path mixer-first receivers as well as FA-based receivers, while numerical results were obtained for other cases. The results agree well with simulations and prior-art. A summary of impedance matching performance of the analyzed circuits is provided in Table II. Guidelines are also provided for proper choice of conversion matrix expressions/sizes in case of numerical computation.

Table II
COMPARISON OF LPTV RECEIVER FRONT-ENDS

Scheme	Mixer-first	Switched-cap with reset	FA-based receiver
Matching mechanism	Upconverted impedance	Switched-cap resistance	Upfront (time-varying) resistor
$Z_{in}(f_{LO}) \approx R_s$ (for current source)	$R_L = (\pi^2/2)R_s$ (4-path)	$C_s \approx 0.63/(Nf_{LO}R_s)$ (N-path)	$mean[R_{in}(t)] = R_s$
$S_{11}(f_{LO}) \approx 0$	$R_L \approx (\pi^2/1.5)R_s$ (4-path)	$C_s \approx 0.63/(Nf_{LO}R_s)$ (N-path)	$mean[\Gamma(t)] \approx 0$ (constrained $R_{in}(t)$)
$S_{11} \approx 0$ bandwidth	Narrowband	Wideband	Wideband
Fraction of power @f_{LO} reradiated	-7dB (4-path) -13dB (8-path)	-7dB (8-path) -8dB (16-path)	$mean\left[\lvert\Gamma(t)\rvert^2\right]$
Reducing reflections	Increase no. of paths	Increase no. of paths	Constrain $R_{in}(t)$/ increase no. of branches, ≈ 0 possible with M=3

APPENDIX A
INPUT IMPEDANCE OF AN IDEAL MIXER-FIRST RECEIVER

Consider an N-path mixer first receiver switching at frequency, ω_p (an example 4-path is shown in Fig. 3). The baseband load impedance, $Z_L(\omega) = 1/Y_L(\omega) = R_L||(1/j\omega C_L)$ has a diagonal conversion matrix, $\mathbb{Z}_L(\omega) = \left[R_L^{-1}\mathbb{I} + jC_L\mathbf{\Omega}(\omega)\right]^{-1}$. Assuming that the baseband bandwidth $1/(R_LC_L) \ll \omega_p$, for a small offset frequency ω ($\omega/\omega_p \ll 1$) $\mathbb{Z}_L(\omega)$ reduces to a 1-element matrix, i.e. $\mathbb{Z}_L(\omega) \approx diag\left\{\left[\begin{array}{ccccc}\cdots & 0 & Z_L(\omega) & 0 & \cdots\end{array}\right]\right\} = \lambda^*\left[Z_L(\omega)\right]\lambda$, where $\lambda = \left[\begin{array}{ccccc}\cdots & 0 & 1 & 0 & \cdots\end{array}\right]$. This simplification applies to any $Z_L(\omega)$ as long as $Z_L(\omega) \approx 0$ for $|\omega| > \omega_p/2$.

The elements of conversion matrix of the switch conductance variation in the n^{th} path ($n \epsilon \{0, 1, 2, 3, ..., N-1\}$), $\mathbb{G}_n$, are found from the Fourier series coefficients of their corresponding conductance variation, $G_n(t) = \sum\limits_{m=-\infty}^{\infty} G_{n,m}e^{jm\omega_p t}$. In case of an ideal mixer-first receiver with switch ON and OFF conductances of G_{on} and G_{off}, respectively,

$$G_{n,m} = \frac{1}{N}\left(G_{on} - G_{off}\right) sinc\left(\frac{m\pi}{N}\right) exp\left(-j\frac{2\pi nm}{N}\right), \quad (20)$$

with $G_{n,0} = \frac{1}{N}(G_{on} - G_{off}) + G_{off}$ (Fourier series coefficients of a $1/N$ duty-cycle square wave switching between $G_{on} = 1/R_{on}$ and G_{off} (usually 0)). It can be noted that $\mathbb{G}_{n+1}$ can be expressed as the Hadamard product[7], $\mathbb{G}_{n+1} = \mathbb{W} \odot \mathbb{G}_n$, where $\mathbb{W} = \underline{W}\,\underline{W}^{-1}$, $\underline{W}$ being the diagonal matrix $diag\left\{\left[\begin{array}{cccccc}1 & w & w^2 & \cdots & \cdots\end{array}\right]\right\}$, with $w = exp\left(-j\frac{2\pi m}{N}\right)$. The Hadamard product operation with $\mathbb{W}$ incorporates the fact that $G_{n+1}(t)$ is simply a phase-delayed version of $G_n(t)$. Interestingly, $\mathbb{W} \odot \mathbb{G}_n$ can also be expressed as $\mathbb{W} \odot \mathbb{G}_n = \underline{W}\mathbb{G}_n\underline{W}^{-1} \Rightarrow (\mathbb{W} \odot \mathbb{G}_n)^{-1} = \underline{W}\mathbb{G}_n^{-1}\underline{W}^{-1} = \mathbb{W} \odot \mathbb{G}_n^{-1}$, i.e. the Hadamard product relationship exists with the inverses as well (intuitive since the resistance-variation $R_{n+1}(t) = 1/G_{n+1}(t)$ is a phase-delayed version of $R_n(t)$). Also, the diagonal entries of $\mathbb{W}$ are 1, meaning $\mathbb{W} \odot \mathbb{Z}_L = \mathbb{Z}_L$. Hence,

$$\left[\mathbb{Z}_L + \mathbb{G}_n^{-1}\right]^{-1} = \mathbb{W} \odot \mathbb{W} \odot \cdots n \text{ times } \odot \left[\mathbb{Z}_L + \mathbb{G}_0^{-1}\right]^{-1}.$$

The conversion matrix of the input admittance of the ideal mixer-first receiver is given by (12) as $\mathbb{Y}_{in}(\omega) = \sum\limits_{n=0}^{N-1}\left[\mathbb{Z}_L + \mathbb{G}_n^{-1}\right]^{-1}$ that simplifies to

$$\mathbb{Y}_{in}(\omega) = \mathbb{P}_N \odot \left[\mathbb{Z}_L + \mathbb{G}_0^{-1}\right]^{-1},$$

where $\mathbb{P}_N = \mathbb{J} + \mathbb{W} + \mathbb{W} \odot \mathbb{W} + \ldots + \mathbb{W} \odot \mathbb{W} \odot \cdots N-1$ times ($\mathbb{J}$ is a matrix of all 1s, i.e. $\mathbb{J} \odot \mathbb{A} = \mathbb{A}\,\forall\,\mathbb{A}$), i.e

$$\mathbb{P}_N = N\left[\begin{array}{cccc} 1 & \frac{1-w^{-N}}{1-w} & \frac{1-w^{-2N}}{1-w} & \cdots \\ \frac{1-w^N}{1-w} & 1 & \ddots & \ddots \\ \frac{1-w^{2N}}{1-w} & \ddots & \ddots & \ddots \\ \vdots & \ddots & \ddots & \ddots \end{array}\right].$$

$\mathbb{P}_N$ simplifies greatly since $w^N = 1$, and so

$$\mathbb{P}_N = N\left[\begin{array}{ccc} \mathbb{I}_N & \mathbb{I}_N & \cdots \\ \mathbb{I}_N & \mathbb{I}_N & \cdots \\ \vdots & \vdots & \ddots \end{array}\right],$$

where $\mathbb{I}_N$ is the $N \times N$ identity matrix. It is notable that the only non-zero terms in $\mathbb{P}_N$ are offset from the matrix diagonal by multiples of N. All subsequent matrix equations involving $\mathbb{P}_N$ can also be shown to have non-zero terms at similar locations, implying that frequency shifts in the circuit are by multiples of $N\omega_p$. This is a known property of perfectly matched N-path circuits with clocks that are exactly delayed by multiples of $1/(N\omega_p)$ [15], [16]. Nevertheless, mismatches can reintroduce frequency shifts from other harmonics of ω_p.

Using, $\mathbb{Z}_L = \lambda^*\left[Z_L(\omega)\right]\lambda$ and the Woodbury matrix identity[8], it can be shown that

$$\begin{array}{rcl}\left[\mathbb{G}_0^{-1} + \mathbb{Z}_L\right]^{-1} & = & \mathbb{G}_0 - \mathbb{G}_0\lambda^*\left[Y_L(\omega) + \lambda\mathbb{G}_0\lambda^*\right]^{-1}\lambda\mathbb{G}_0 \\ & = & \mathbb{G}_0 - \mu^*\left[Y_L(\omega) + G_{0,0}\right]^{-1}\mu,\end{array}$$

where $\mu = \left[\begin{array}{ccccc}\cdots & G_{0,1} & G_{0,0} & G_{0,-1} & \cdots\end{array}\right]$ is the middle row of $\mathbb{G}_0$. Hence, $\mathbb{Y}_{in}(\omega) = \mathbb{P}_N \odot \left[\mathbb{G}_0 - \mu^*\left[Y_L(\omega) + G_{0,0}\right]^{-1}\mu\right]$. It may be noted that $G_{0,mN} = 0\,\forall\,m \neq 0$ (from (18)). Thus, $\mathbb{P}_N \odot \mathbb{G}_0 = NG_{0,0}\mathbb{I}$. Further, it can be verified that $\mathbb{P}_N \odot \mu^*\mu = N\sigma^*\sigma$, where

$$\sigma = \left[\begin{array}{cccccc} G_{0,K} & 0 & \cdots & 0 & G_{0,K-N} & \cdots \\ 0 & G_{0,K-1} & \ddots & \vdots & 0 & \cdots \\ \vdots & \ddots & \ddots & 0 & \vdots & \cdots \\ 0 & \cdots & 0 & G_{0,K-N+1} & 0 & \cdots \end{array}\right]$$

[7]The Hadamard product of two $m \times n$ matrices $\mathbb{A}$ and $\mathbb{B}$ is defined by $[\mathbb{A} \odot \mathbb{B}]_{ij} = [\mathbb{A}]_{ij}\,[\mathbb{B}]_{ij}\;\forall\,1 \leq i \leq m,\, 1 \leq j \leq n$.

[8]$[\mathbb{A} + \mathbb{BCD}]^{-1} = \mathbb{A}^{-1} - \mathbb{A}^{-1}\mathbb{B}\left[\mathbb{C}^{-1} + \mathbb{D}\mathbb{A}^{-1}\mathbb{B}\right]^{-1}\mathbb{D}\mathbb{A}^{-1}$.

is an $N \times (2K+1)$ matrix. Thus,

$$\mathbb{Y}_{in}(\omega) = NG_{0,0}\mathbb{I} - N\sigma^* \left[Y_L(\omega) + G_{0,0}\right]^{-1} \sigma. \tag{21}$$

The diagonal elements of the matrix $\mathbb{Y}_{in}(\omega)$ gives the input admittance of the mixer-first receiver. Specifically, the element at $(K+1+k, K+1+k)$ represents the admittance presented by the mixer-first receiver at a frequency of $k\omega_p+\omega$ when driven by an ideal voltage source, denoted by $Y_{V-D}(k\omega_p+\omega)$. Thus, for $G_{off} = 0$

$$\begin{aligned} Y_{V-D}(k\omega_p+\omega) &= NG_{0,0} - \frac{N|G_{0,k}|^2}{Y_L(\omega)+G_{0,0}} \\ &= G_{on}\left[1 - \frac{G_{on}}{G_{on}+NY_L(\omega)} sinc^2\left(\frac{k\pi}{N}\right)\right]. \end{aligned} \tag{22}$$

For large values of G_{on}, i.e. small R_{on}, the input admittance is not strongly dependent on the baseband impedance. This is expected when the receiver is voltage-driven.

Now, $\mathbb{Z}_{in}(\omega) = \mathbb{Y}_{in}^{-1}(\omega)$. It can again be computed using Woodbury matrix identity as $\mathbb{Z}_{in}(\omega) = \frac{1}{NG_{0,0}}\mathbb{I} + \frac{1}{NG_{0,0}^2}\sigma^* \left[Y_L(\omega) + G_{0,0} - \frac{1}{G_{0,0}}\sigma\sigma^*\right]^{-1} \sigma$. $\sigma\sigma^*$ is an $N \times N$ diagonal matrix given by $\sigma\sigma^* = diag\left\{\left[\sum_{k=0}^{\lfloor 2K/N \rfloor} |G_{0,K-kN}|^2 \quad \sum_{k=0}^{\lfloor 2K/N \rfloor} |G_{0,K-kN-1}|^2 \quad \cdots\right]\right\}$. For $G_{off} = 0$, each term in $\sigma\sigma^*$ is of the form $G_{0,0}^2 \sum_{k=-\infty}^{\infty} sinc^2(k\pi+\theta)$ as $K \to \infty$ (using (20)). Since $\sum_{k=-\infty}^{\infty} sinc^2(k\pi+\theta) = 1 \,\forall\, \theta$, $\sigma\sigma^* = G_{0,0}^2\mathbb{I}$, and so $\mathbb{Z}_{in}(\omega)$ simplifies to

$$\mathbb{Z}_{in}(\omega) = \frac{1}{NG_{0,0}}\mathbb{I} + \frac{Z_L(\omega)}{NG_{0,0}^2}\sigma^*\sigma. \tag{23}$$

The diagonal elements of the matrix $\mathbb{Z}_{in}(\omega)$ gives the input impedance of the mixer-first receiver. Specifically, the element at $(K+1+k, K+1+k)$ represents the impedance presented by the mixer-first receiver at a frequency of $k\omega_p+\omega$ when driven by an ideal current source, denoted by $Z_{C-D}(k\omega_p+\omega)$. Thus,

$$\begin{aligned} Z_{C-D}(k\omega_p+\omega) &= \frac{1}{NG_{0,0}} + \frac{Z_L(\omega)|G_{0,k}|^2}{NG_{0,0}^2} \\ &= R_{on} + \frac{1}{N} sinc^2\left(\frac{k\pi}{N}\right) Z_L(\omega). \end{aligned} \tag{24}$$

The input impedance is clearly dominated by the baseband impedance. The result obtained matches prior art [9], [10], where $\Gamma_{N,k} = \frac{1}{N} sinc^2\left(\frac{k\pi}{N}\right)$ denotes the factor by which the baseband impedance is upconverted to frequency, $k\omega_p$.

Finally, consider the case when the receiver is driven by a purely resistive source with source resistive, $R_s = 1/G_s$, i.e. whose conductance conversion matrix is given by $\mathbb{Y}_s(\omega) = G_s\mathbb{I}$. Then the $\mathbb{S}_{11}(\omega)$ matrix is given from (8) by

$$\mathbb{S}_{11}(\omega) = \left[\mathbb{Y}_s(\omega) - \mathbb{Y}_{in}(\omega)\right]\left[\mathbb{Y}_s(\omega) + \mathbb{Y}_{in}(\omega)\right]^{-1}.$$

Matrices $[\mathbb{Y}_s(\omega) - \mathbb{Y}_{in}(\omega)]$ and $[\mathbb{Y}_s(\omega) + \mathbb{Y}_{in}(\omega)]^{-1}$ are easily obtained from (21) and are given by:

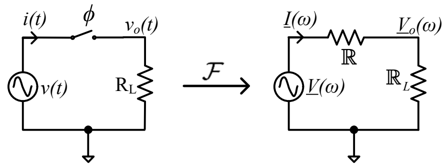

Figure 21. A simple switching circuit

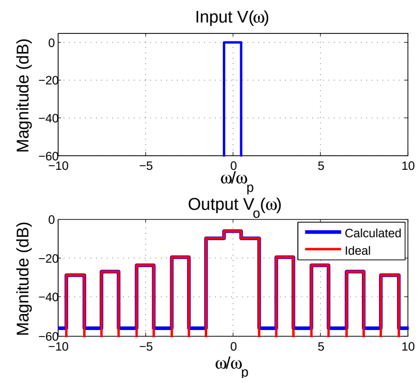

Figure 22. Response of the circuit in Fig. 21 to an input only around DC

$$\begin{aligned} \left[\mathbb{Y}_s(\omega) - \mathbb{Y}_{in}(\omega)\right] &= (G_s - NG_{0,0})\mathbb{I} + \frac{N}{Y_L(\omega)+G_{0,0}}\sigma^*\sigma \\ \left[\mathbb{Y}_s(\omega) + \mathbb{Y}_{in}(\omega)\right]^{-1} &= \frac{1}{G_s+NG_{0,0}} \times \\ &\quad \left[\mathbb{I} + \frac{N}{(G_s+NG_{0,0})Y_L(\omega)+G_sG_{0,0}}\sigma^*\sigma\right] \end{aligned}$$

Now any element of $\mathbb{S}_{11}(\omega)$ can be easily obtained using the relations: $\sigma\sigma^* = G_{0,0}^2\mathbb{I}$ and $N\sigma^*\sigma = \mathbb{P}_N \odot \mu^*\mu$. For example, the element at $(K+1+i, K+1+j)$, i.e. $\gamma_{i,j}(\omega)$ as per (9), can be found by taking the vector dot product between the $(K+1+i)^{th}$ row and the $(K+1+j)^{th}$ column of $[\mathbb{Y}_s(\omega) - \mathbb{Y}_{in}(\omega)]$ and $[\mathbb{Y}_s(\omega) + \mathbb{Y}_{in}(\omega)]^{-1}$, respectively. The elements of $\mathbb{S}_{11}(\omega)$ are computed and on simplification gives (25). Note that $\gamma_{i,j}(\omega) = 0 \,\forall\, (i-j) \neq mN, m \,\epsilon\, \mathbb{Z}$ is a natural consequence of the Hadamard product with $\mathbb{P}_N$ propagating through all the matrix equations.

Of particular interest are the diagonal elements of $\mathbb{S}_{11}(\omega)$ that give the S_{11} of the circuit, i.e. $\gamma_{k,k}(\omega) = S_{11}(k\omega_p+\omega)$. The equivalent impedance corresponding to the obtained S_{11} can be found as shown in (26). This is the impedance presented by the mixer-first receiver to a source with impedance R_s at a frequency of $k\omega_p+\omega$ and is denoted by $Z_{Rs-D}(k\omega_p+\omega)$. Thus, the impedance characteristics of the ideal mixer-first receiver with a memoryless source is completely characterized by (21)-(26).

Appendix B
Convergence of Results with Matrix Size

Consider the simple LPTV circuit shown in Fig. 21 wherein a voltage source drops its potential across a series combination of a constant load resistor and a switch that is periodically turned ON and OFF with clock ϕ of frequency, ω_p. The switch can be modeled as an LPTV resistor with a resistance variation, $R(t)$ and conversion matrix, $\mathbb{R}$, while the constant

$$\gamma_{i,j}(\omega)=\begin{cases}\frac{G_s-NG_{0,0}}{G_s+NG_{0,0}}+\frac{2NG_s|G_{0,k}|^2}{(G_s+NG_{0,0})[(G_s+NG_{0,0})Y_L(\omega)+G_sG_{0,0}]} & j=i\\ \frac{2NG_sG_{0,i}G_{0,-j}}{(G_s+NG_{0,0})[(G_s+NG_{0,0})Y_L(\omega)+G_sG_{0,0}]} & j=i+mN,\ m\,\epsilon\,\mathbb{Z}-\{0\}\\ 0 & else\end{cases}$$

$$=\begin{cases}\frac{R_{on}-R_s}{R_{on}+R_s}+\frac{2R_s sinc^2\left(\frac{i\pi}{N}\right)Z_L(\omega)}{(R_{on}+R_s)[Z_L(\omega)+N(R_{on}+R_s)]} & j=i\\ \frac{2R_s sinc\left(\frac{i\pi}{N}\right)sinc\left(\frac{j\pi}{N}\right)Z_L(\omega)}{(R_{on}+R_s)[Z_L(\omega)+N(R_{on}+R_s)]} & j=i+mN,\ m\,\epsilon\,\mathbb{Z}-\{0\}\\ 0 & else\end{cases} \tag{25}$$

$$Z_{Rs-D}(k\omega_p+\omega)=R_s\frac{1+S_{11}(k\omega_p+\omega)}{1-S_{11}(k\omega_p+\omega)}=R_{on}+\frac{(R_{on}+R_s)\,sinc^2\left(\frac{k\pi}{N}\right)Z_L(\omega)}{N\,(R_{on}+R_s)+\left[1-sinc^2\left(\frac{k\pi}{N}\right)\right]Z_L(\omega)}. \tag{26}$$

load resistance has a conversion matrix, $\mathbb{R}_L=R_L\mathbb{I}$. Then the output voltage can be deduced readily as:

$$\underline{V_o}(\omega)=\mathbb{R}_L\underline{I}(\omega)=\mathbb{R}_L\left[\mathbb{R}+\mathbb{R}_L\right]^{-1}\underline{V}(\omega). \tag{27}$$

Given component values based on the clock waveform, the expression can be evaluated numerically to find the output of the circuit. For example, for an ideal 50% duty-cycle ϕ, with switch ON and OFF resistances of $R_{on}=1\Omega$ and $R_{off}=10k\Omega$, with $R_L=100\Omega$, the calculated magnitude of $V_o(\omega)$ is plotted in Fig. 22 for $K=500$. From the plot, it is clear that the calculated output matches the ideal values around odd harmonics of ω_p, while for even harmonics the result is not exactly zero as expected (but still small). The convergence of the output magnitude of $V_o(\omega)$ around the 0^{th}, 1^{st}, 2^{nd} and 9^{th} harmonics of ω_p are plotted as A_0, A_1, A_2, and A_9, respectively, with conversion matrix size, i.e. K is plotted in Fig. 23. As is evident, the DC and odd harmonics (up to 9) converge for about $K=100$, while the even harmonics, ideally absent, reduce steadily with increasing K.

Can the convergence be made faster? In (27), $\underline{I}(\omega)$ is valued as $\left[\mathbb{R}+\mathbb{R}_L\right]^{-1}\underline{V}(\omega)$, i.e. the inverse conversion matrix of sum of $R(t)$ and R_L. Instead, if $G_T(t)=1/\left[R(t)+R_L\right]$ is used to build a corresponding matrix, $\mathbb{G}_T$, then $\underline{I}(\omega)=\mathbb{G}_T\underline{V}(\omega)$. It can be shown that the output

$$\underline{V_o}(\omega)=\mathbb{R}_L\underline{I}(\omega)=\mathbb{R}_L\mathbb{G}_T\underline{V}(\omega) \tag{28}$$

for frequencies up to $\pm M\omega_p$ matches the ideal value for $K=M$, i.e. much faster than with (27). In fact, the even harmonic terms are exactly 0.

Why does (28) converge much faster than (27)? The reason is that the matrix inversion, $\left[\mathbb{R}+\mathbb{R}_L\right]^{-1}$ converges to its ideal value, $\mathbb{G}_T$, only as $K\to\infty$ (convergence can be proved using Lemma 4.5 in [23]). This is because $G_T(t)$ is related to $\left[R(t)+R_L\right]$ by an inverse (an extremely non-linear function). Thus, the frequency content in $G_T(t)$ within $[-M\omega_p,M\omega_p]$ is not only dependent on frequency content within $[-M\omega_p,M\omega_p]$ in $\left[R(t)+R_L\right]$, but a much larger frequency range (or equivalently a larger K). As an example, consider $R(t)=1+a\,sin(\omega_pt)$ $|a|<1$, i.e. a single-tone sinusoid. To represent $G(t)=1/R(t)$ accurately with at least 99% of its power, the no. of harmonics, K, necessary is plotted in Fig. 24 as a function of a. $K\sim 1/\left(1-|a|\right)$ is clearly greater than 1 for a large range of a.

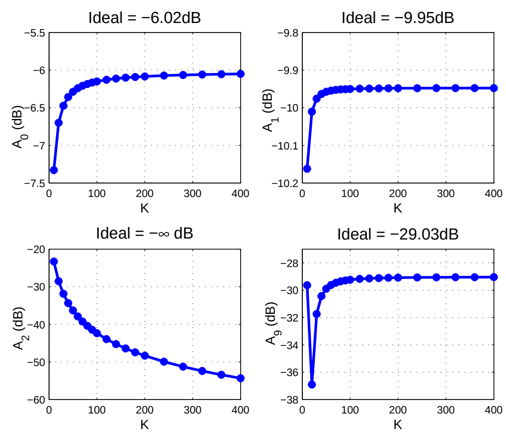

Figure 23. Convergence of amplitude of the output around the n^{th} harmonic, A_n, with matrix size, K, in the analysis

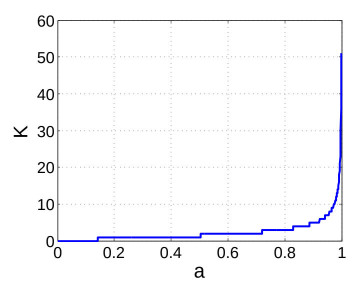

Figure 24. No. of harmonics, K, needed to represent $G(t)=1/\left[1+a\,sin(\omega_pt)\right]$ with 99% of its total power

The above observations can be used to establish some guidelines regarding matrix size, i.e., K:

1) Replace matrix inverses with more accurate versions if possible, for example $\left[\mathbb{R}+\mathbb{R}_L\right]^{-1}$ with $\mathbb{G}_T$ in (28). This avoids introducing errors due to finite-dimensioned matrix inverses.
2) Representation of time-varying elements must to chosen to minimize matrix inversions. For example, in the mixer-first receiver analysis in Appendix A, the switches are represented by conductances instead of resistances to reduce inversions in the analysis.
3) If inversions cannot be avoided, choose K such that the matrices represent both the underlying LPTV component variation, and its inverse with enough precision. For

example, while representing $R(t)$ with a conversion matrix, $\mathbb{R}$, K must be chosen so that the Fourier series representations of both $R(t)$ and $1/R(t)$ includes, say, 99% (depending on required accuracy) of their total power.

REFERENCES

[1] El Oualkadi, A.; El Kaamouchi, M.; Paillot, J.-M.; Vanhoenacker-Janvier, D.; Flandre, D., "Fully Integrated High-Q Switched Capacitor Bandpass Filter with Center Frequency and Bandwidth Tuning," *Radio Frequency Integrated Circuits (RFIC) Symposium, 2007 IEEE* , vol., no., pp.681,684, 3-5 June 2007.

[2] Ghaffari, A.; Klumperink, E.A.M.; Soer, M. C M; Nauta, B., "Tunable High-Q N-Path Band-Pass Filters: Modeling and Verification," *Solid-State Circuits, IEEE Journal of* , vol.46, no.5, pp.998,1010, May 2011.

[3] Andrews, C.; Molnar, A.C., "Implications of Passive Mixer Transparency for Impedance Matching and Noise Figure in Passive Mixer-First Receivers," *Circuits and Systems I: Regular Papers, IEEE Transactions on* , vol.57, no.12, pp.3092,3103, Dec. 2010.

[4] Andrews, C.; Molnar, A.C., "A Passive Mixer-First Receiver With Digitally Controlled and Widely Tunable RF Interface,"*Solid-State Circuits, IEEE Journal of* , vol. 45, no. 12, pp. 2696-2708, Dec. 2010.

[5] D. Yang, et al., "Optimized Design of N-Phase Passive Mixer-First Receivers in Wideband Operation," *Circuits and Systems I: Regular Papers, IEEE Transactions on* , vol. 62, no. 11, pp. 2759-2770, Nov. 2015.

[6] Murphy, D., et al., "A Blocker-Tolerant, Noise-Cancelling Receiver Suitable for Wideband Wireless Applications," in *Solid-State Circuits, IEEE Journal of* , vol.47, no.12, pp.2943-2963, Dec. 2012.

[7] Hameed, S, et al., "A programmable receiver front-end achieving >17dBm IIP3 at <1.25×BW frequency offset", *Solid-State Circuits Conference Digest of Technical Papers (ISSCC), 2016 IEEE International* , vol., no., pp.446,447, 31 Jan.-4 Feb. 2016.

[8] Hameed, S.; Pamarti, S., "A time-interleaved filtering-by-aliasing receiver front-end with >70dB suppression at <4×bandwidth frequency offset", *Solid-State Circuits Conference Digest of Technical Papers (ISSCC), 2017 IEEE International* , vol., no., pp.418,419, 4-8 Feb. 2017.

[9] Mirzaei, A.; Darabi, H.; Leete, J.C.; Yuyu Chang, "Analysis and Optimization of Direct-Conversion Receivers With 25% Duty-Cycle Current-Driven Passive Mixers," *Circuits and Systems I: Regular Papers, IEEE Transactions on* , vol.57, no.9, pp.2353,2366, Sept. 2010.

[10] Mirzaei, A.; Darabi, H., "Analysis of Imperfections on Performance of 4-Phase Passive-Mixer-Based High-Q Bandpass Filters in SAW-Less Receivers," *Circuits and Systems I: Regular Papers, IEEE Transactions on* , vol.58, no.5, pp.879,892, May 2011.

[11] Strom, T.; Signell, S., "Analysis of periodically switched linear circuits," *Circuits and Systems, IEEE Transactions on* , vol.24, no.10, pp.531,541, Oct 1977.

[12] Soer, M. C M; Klumperink, E.A.M.; de Boer, P.-T.; van Vliet, F.E.; Nauta, B., "Unified Frequency-Domain Analysis of Switched-Series- RC Passive Mixers and Samplers," *Circuits and Systems I: Regular Papers, IEEE Transactions on* , vol.57, no.10, pp.2618,2631, Oct. 2010.

[13] Xu, Y., et al., " A Switched-Capacitor RF Front End With Embedded Programmable High-Order Filtering,"in *Solid-State Circuits, IEEE Journal of* , vol.51, no.5, pp.1154-1167, May 2016.

[14] Iizuka, T.; Abidi, A.A., "FET-R-C Circuits: A Unified Treatment—Part I: Signal Transfer Characteristics of a Single-Path," *Circuits and Systems I: Regular Papers, IEEE Transactions on* , vol. 63, no. 9, pp. 1325-1336, Sept. 2016.

[15] Iizuka, T.; Abidi, A.A., "FET-R-C Circuits: A Unified Treatment—Part II: Extension to Multi-Paths, Noise Figure, and Driving-Point Impedance," *Circuits and Systems I: Regular Papers, IEEE Transactions on* , vol. 63, no. 9, pp. 1337-1348, Sept. 2016.

[16] Pavan, S.; Klumperink, E., "Simplified Unified Analysis of Switched-RC Passive Mixers, Samplers, and N -Path Filters Using the Adjoint Network," *Circuits and Systems I: Regular Papers, IEEE Transactions on* , vol. 64, no. 10, pp. 2714-2725, Oct. 2017.

[17] Pavan, S.; Klumperink, E., "Analysis of the Effect of Source Capacitance and Inductance on N-Path Mixers and Filters," *Circuits and Systems I: Regular Papers, IEEE Transactions on* , vol. PP, no. 99, pp. 1-12.

[18] S. A. Maas, *Nonlinear microwave and RF circuits*, 2nd Ed., Artech House, 2003.

[19] Hameed, S., et al., "Frequency-domain analysis of a mixer-first receiver using conversion matrices", *Circuits and Systems (ISCAS), 2015 IEEE International Symposium on* , vol., no., pp.541,544, 24-27 May 2015.

[20] Hameed, S., et al., "Frequency-Domain Analysis of N-path Filters Using Conversion Matrices," *Circuits and Systems II: Express Briefs, IEEE Transactions on* , vol.63, no.1, pp.74-78, Jan. 2016.

[21] Kundert, K.S.; Sangiovanni-Vincentelli, A, "Simulation of Nonlinear Circuits in the Frequency Domain," *Computer-Aided Design of Integrated Circuits and Systems, IEEE Transactions on* , vol.5, no.4, pp.521,535, October 1986.

[22] Brachtendorf, H.G.; Welsch, G.;Laur, R., "Fast simulation of the steady-state of circuits by the harmonic balance technique," *Circuits and Systems (ISCAS), 1995 IEEE International Symposium on*, Seattle, WA, 1995, pp. 1388-1391 vol.2.

[23] Robert M. Gray (2006), "Toeplitz and Circulant Matrices: A Review", Foundations and Trends® in Communications and Information Theory: Vol. 2: No. 3, pp 155-239. http://dx.doi.org/10.1561/0100000006

[24] M. Rachid, et al., "Filtering by Aliasing," *in Signal Processing, IEEE Transactions on* , vol.61, no.9, pp.2319-2327, May1, 2013.

[25] Hameed, S.; Pamarti, S., "Design and Analysis of a Programmable Receiver Front End Based on Baseband Analog-FIR Filtering Using an LPTV Resistor," *Solid-State Circuits, IEEE Journal of* , vol. PP, no. 99, pp. 1-15.

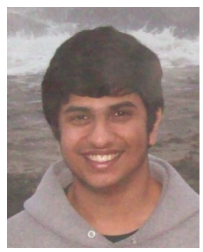

Sameed Hameed (S'13–M'17) received the B.Tech. degree from IIT Madras, India, in 2011, and the M.S. and the Ph.D. degrees from the University of California, Los Angeles (UCLA), CA, USA, in 2013 and 2017, respectively, all in electrical engineering.

In 2013, he joined Broadcom, Irvine, CA, USA, as an RFIC Design Intern. From 2016 to 2017, he was an RFIC Design Intern at Silvus Technologies, Los Angeles, CA, USA, where he is currently an RFIC Engineer. His current research interests include RF transceiver designs with an emphasis on signal processing techniques.

Dr. Hameed was a recipient of an Electrical Engineering Department Fellowship in 2013 for placing first in the 2013 Ph.D. preliminary exam in circuits and embedded systems, a UCLA Graduate Division Fellowship in 2014, the Broadcom UCLA Fellowship during the 2015–2016 academic year, the Dissertation Year Fellowship and the MediaTek UCLA Fellowship during the 2016–2017 academic year, the IEEE SSCS 2015–2016 PreDoctoral Achievement Award, the 2016–2017 SSCS Student Travel Grant, and the UCLA Electrical Engineering Department's 2016-2017 Distinguished Ph.D. Dissertation in Circuits and Embedded Systems Award.

Sudhakar Pamarti (S'98–M'03) received the B.Tech. degree in electronics and electrical communication engineering from IIT Kharagpur, India, in 1995, and the M.S. and the Ph.D. degrees in electrical engineering from the University of California, San Diego, CA, USA, in 1999 and 2003, respectively.

From 1995 to 1997, he was at Hughes Software Systems, New Delhi, India, and from 2003 to 2005, he was at Rambus Inc., Sunnyvale, CA, USA, developing embedded software and firmware for a wireless communication system, and high-speed I/O circuits, respectively. He is currently a Professor of electrical and computer engineering with the University of California, Los Angeles, CA, USA. His current research interests include integrated circuit designs with special focus on developing algorithmic techniques to overcome circuit impairments.

Dr. Pamarti was a recipient of the National Science Foundation's CAREER Award. He has served as an Associate Editor for both the IEEE TRANSACTIONS ON CIRCUITS AND SYSTEMS I AND II. He currently serves on the Technical Program Committee of the IEEE Custom Integrated Circuits Conference and the IEEE International Solid-State Circuits Conference.